Hydrogen, Fuel Cell & Energy Storage 10 (2023) 1-10

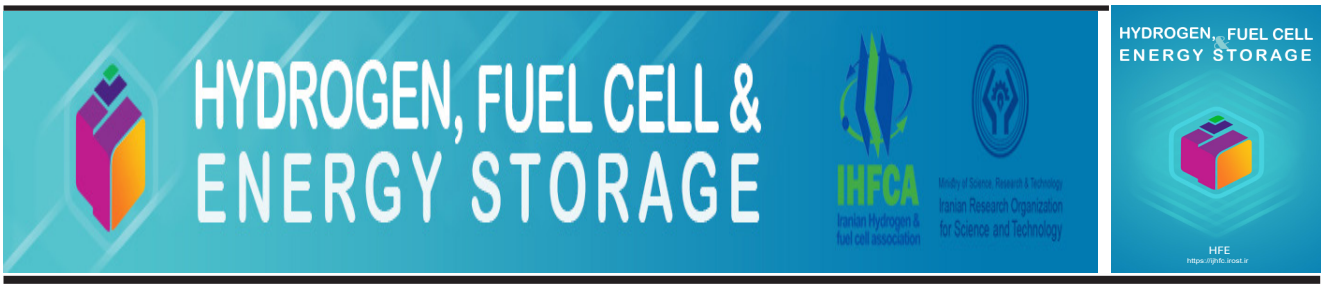

Preparation, characterization, and the study of the electrochemical behavior of Y-doped Bariumcerate powders by new precursors

S. Ghamari, M. Ranjbar*

Department of Chemical Technologies, Iranian Research Organization for Science and Technology (IROST), Tehran, Iran

Article Information

Article History:

Received:
14 Aug 2022
Received in revised form:
07 Oct 2022
Accepted:
17 Oct 2022

Keywords

Solid oxide fuel cell
Photonics conducting mebrane
Yttrium doped barium cerate
Soft chemistry method

Abstract

Proton ion conducting nano crystalline yttrium doped barium cerate (YBCO) is synthesized by ethylene glycol using the citric acid assisted sol–gel method. In this paper, two different kinds of $BaCe_{0.9}Y_{0.1}O_{3-a}$ nanocomposites were prepared. YBCO (I) was synthesized by $[(Ce_2(pydc)_4(H_2O)_4].pyda.H]_2.2H_2O$, $\{[Ba_{1.5}$ (pydc.H) (pydc) (H_2O)]. H_2O. 0.5 $(pydc.H_2)\}_n$, $[(Y_2$ $(pydc)_4$ $(H_2O)_4].pyda.H]_2.2H_2O]]$, [pydc (2,6-Pyridinedicarboxylic acid), pyda (2,6-diaminopyridine)] and YBCO (II) was synthesized by $(Y(NO_3)_2.6H_2O$, $Ba(NO_3)_2$, $Ce(NO_3).6H_2O)$. The (I) and (II) powders were calcined for a period of 8 hours at 900 °C to get fine yttrium-doped barium cerate powders, and then the specifications were compared. Various analytical techniques have been used to characterize the samples, such as scanning electron microscope (SEM), Energy-Dispersive X-ray Spectroscopy (EDS), thermal analysis TG/DTA, and X-ray powder diffraction (XRD). The results showed that the powders synthesized by metal complexes containing LH_2 ligands as precursors were denser and more homogeneous with smaller particle sizes. The experimental results showed that YBCO (I) effectively improved the electrochemical performance of the electrolyte.

1. Introduction

A solid oxide fuel cell, SOFC, is an electrochemical conversion device that produces electricity directly from oxidizing a fuel. Yttria stabilized Zirconia (YSZ) is the most commonly used electrolyte in SOFCs; it requires an operating temperature between 700-900 °C to ensure sufficient oxygen ion conductivity [1]. Among the various electrolytes, proton ion

*Corresponding Author:ma¬randjbar@irost.ir (M.Ranjbar)

doi: 10.22104/IJHFC.2022.5799.1243

conductors are the most promising compared to oxygen ion conductors because of their relatively higher ionic conductivity and lower activation energy in this temperature range [1]. Protonic conducting membranes with a perovskite-type structure have been studied for hydrogen separation for many years [2]. The ionic section of the conductivity occurs by anion motion via the vacancy mechanism. Proton-conducting perovskite-type oxides were first described by Iwahara in 1981 [2]. Many oxides, most with perovskite structures, show proton ion conductivity and the ability to absorb proton ions [1], and many studies have focused on the electrical conductivity of $BaCeO_3$-based ceramics. $BaCeO_3$ crystallizes in the perovskite structure and exhibits three-phase transitions up to 1000 °C. The first transition at 290 °C leads from a primitive orthorhombic perovskite structure (space group: Pmcn) to a body-centered one (Incn), a second transition at 400 °C leads to a rhombohedrally distorted one (R3c), and the last transition at 900 °C leads to the cubic perovskite structure (Pm3m) [3]. However, sintering temperatures above 1500 °C should be avoided because $BaCeO_3$ melts with the formation of CeO_2 and a liquid containing BaO [3]. Several synthesis procedures have been suggested in the literature for the preparation of barium cerate materials [4], including solid-state [5], glycine nitrate combustion [6], sol-gel [7], and pechini [8] methods. All these methods have their advantages and disadvantages. The mentioned sol–gel method using metal complexes as precursors is a unique combination of a thermal process and a chemical chelation process, but its disadvantage includes the problem of controlling the rate of hydrolysis of different metal oxides in the sol-gel process [9]. In this research work, two different kinds of YBCO (I and II) were prepared with a new precursor using the sol-gel method. YBCOs (I) and (II) powders were prepared with new yttrium, barium, cerium complexes, and nitrate salts of yttrium, barium, and cerium, respectively. The sol–gel synthesis routes use ethylene glycol (EG) and citric acid (CA) as complexing agents and fuels. Finally, the two different kinds of as-synthesized YBCOs (I) and (II) powders were characterized and compared to each other. The electrochemical behavior of YBCO (I) was also compared with YBCO (II).

2. Experimental

2.1 Materials and equipment

All reagents and solvents for synthesis and analysis were commercially available and were used as received. Chemicals and solvents were purchased from Merck. All solutions were prepared using double distilled water. The melting points were measured with a Thermo Scientific 9200 apparatus. Fourier transform infrared (FTIR) spectra were recorded on a Bruker tensor 27 spectrometer in the range 400–4000 cm^{-1} using the KBr disk technique. A phase of the sintered samples was analyzed by XRD on a Philips diffractometer from X-pert companies with Cu-Kα radiation (λ=1.54 Å). Particle size analysis of the powder was measured using a nano sizer Scanning Electron Microscope (SEM) along with Energy-dispersive X-ray Spectroscopy (EDS) on a Zeiss apparatus. Thermogravimetric analysis (TGA) and differential thermal analyses (DTA) of the title compound were performed on a computer-controlled D-32609 Hüllhorst apparatus. Thermo gravimetric and compounds were heated in a nitrogen atmosphere from 10-600 °C samples at a heating rate of 10 °C/min. Furthermore, a multiwave ultrasonic generator (UP600S, Mosonix) equipped with a converter/transducer and titanium oscillator (horn), 12.5 mm in diameter, operating at 20 kHz with a

maximum power output of 600 W was used for ultrasonic irradiation. Powder samples YBCO (I) and (II) were loaded into alumina pans and heated at a ramp rate of 10 °C/min from room temperature to 900 °C under an argon atmosphere.

2.2. Preparation of nano-structured Y(III), Ba(II), and Ce(III) Complexes

The LH_2 ligand, $[pyda.H_2]^{2+}[pydc]^{2-}$, was prepared according to the literature procedure [10, 11]. To prepare the nano structures of $[(Ce_2(pydc)_4(H_2O)_4].pyda.H]_2.2H_2O$, $\{[Ba_{1.5}(pydc.H)(pydc)(H_2O)].H_2O.0.5(pydc.H_2)\}_n$ and $[(Y_2(pydc)_4(H_2O)_4].pyda.H]_2.2H_2O]]$, compounds, the metal nitrates such as $Y(NO_3)_2.6H_2O$ (1mmol), $Ba(NO_3)_2$ (1mmol), and $Ce(NO_3)6.H_2O$ (1mmol), respectively, were dissolved in a mixture of 70:30 Methanol:H_2O separately. LH_2 ligand with different mole ratios (Table 1) was dissolved separately in a solvent of 70:30 Methanol:H_2O, respectively. Both were placed in a high-density ultrasonic probe vessel operating at 20 kHz with a maximum power output of 600 W. After 1 hour, a suspension was formed for three complexes. The powders were isolated by centrifugation (4000 rpm, 15 min), washed with water and acetone, and finally dried in air.

Table. 1 Values of LH2 ligand for the synthesis of complexes.

complex	LH_2 values (mmol)
$[(Ce_2(pydc)_4(H_2O)_4].pyda.H]_2.2H_2O$	3
$\{[Ba_{1.5}(pydc.H)(pydc)(H_2O)].H_2O.0.5(pydc.H_2)\}_n$	2
$[(Y_2(pydc)_4(H_2O)_4].pyda.H]_2.2H_2O]]$	3

2.3 Preparation of YBCO (I) and (II) nano composites by the sol-gel method, $Y_{0.1}BaCe_{0.9}O_3$ (YBC10)

The nano particles of YBCO (I and II) was prepared by a wet-chemical method based on the sol–gel process with new precursors. The composite of YBCO (I) was prepared by new yttrium, barium, and cerium complexes, and YBCO (II) was synthesized by $Y(NO_3)_2.6H_2O$ (1 mmol), $Ba(NO_3)_2$ (10 mmol), and $Ce(NO_3)6.H_2O$ (9 mmol) using the sol-gel reaction. The Y(III) complex, $[(Y_2(pydc)_4(H_2O)_4].pyda.H]_2.2H_2O]]$ ((1 mmol), Ba(II) complex, $\{[Ba_{1.5}(pydc.H)(pydc)(H_2O)].H_2O.0.5(pydc.H_2)\}_n$, (10 mmol), and Ce(III) complex, $[(Ce_2(pydc)_4(H_2O)_4].pyda.H]_2.2H_2O$, (9 mmol) as precursors were dissolved in deionized water, followed by the addition of Ethylene glycol and citric acid as polymerizing agents and fuels dissolved in deionized water. After homogenization of this solution, the temperature was raised to 90 °C, while the solution was constantly stirred for 4 h. Then, the obtained gel was cooled down to room temperature, and the dried powders were calcined for a period of 8 hours at 900 °C at the rate of thermal treatment 5 °C/min to get fine yttrium doped barium cerate powders. The powders were then characterized using FT-IR, XRD, SEM, EDAX and TG/DTA techniques. Finally, the electrochemical performance was characterized by the electrochemical impedance spectroscopy (EIS) technique using a VMP-3 multi-channel potentiostat in the frequency range of 0.1 Hz to 0.1 MHz and a signal amplitude of 10 mV at 650-800 °C.

3. Results and discussion

Two different kinds of YBCO compounds, (I) and (II), were synthesized by a soft chemistry method based on the sol–gel process. Fig. 1 shows the FT-IR spectra

of a) LH2 ligand $[pyda.H_2]^{2+}[pydc]^{2-}$, b) Y(III) complex $[(Y_2(pydc)_4 (H_2O)_4].pyda.H]_2.2H_2O]]$, c) Ba(II) complex $\{[Ba_{1.5}(pydc.H)(pydc)(H_2O)].H_2O.\ 0.5(pydc.H_2)\}_n$, and d) Ce(III) complex $[(Ce_2(pydc)_4(H_2O)_4].pyda.H]_2.2H_2O$, respectively. The signals at ~ 1640 and ~ 1360 cm^{-1} for carboxylate coordination and ~ 780 and ~ 635 cm^{-1} are due to the pyridine coordination bond vibrations [12]. A comparison between the FTIR spectrum of free LH_2 ligand and its Ce(III), Ba(II), and Y(III) complexes obviously revealed that the ligand had been coordinated to Ce(III), Ba(II), and Y(III) ions, and new compounds were formed. A distinct carbonyl peak υ (COOH) around 1670 cm^{-1} in free LH_2 has been shifted to 1595 cm^{-1}. New bands appeared in the FT-IR spectrum of Ce(III), Ba(II), and Y(III) complexes resulting from the new metal–ligand (M–N and M–O) bond formations. These bands are positioned at ~ 492 and 558 cm^{-1}. The powders were stuck by Vander Waals forces of attraction and led to the formation of comparatively large clusters. Therefore, based on these results, the chemical formula suggested for the LH2 ligand $[pyda.H_2]^{2+}[pydc]^{2-}$, the Y(III) complex $[(Y_2(pydc)_4(H_2O)_4].pyda.H]_2.2H_2O]]$, Ba(II) complex $\{[Ba_{1.5}(pydc.H)(pydc)(H_2O)].H_2O.\ 0.5(pydc.H_2)\}_n$, and Ce(III) complex $[(Ce_2(pydc)_4(H_2O)_4].pyda.H]_2.2H_2O$, the existing of pydc and pyda moieties, and metal-N, metal-O vibration bonding have been confirmed.

The X-ray diffraction patterns of the as-prepared two different kinds of YBCO (I) and (II) powders are shown in Fig. 2. This figure confirms that YBCO powders prepared by the sol-gel reaction method can achieve their perovskite structure, interpreted as rhombohedral (space group: R3c) [13, 14]. Moreover, the YBCO X-ray patterns influence not only the phase composition and crystallographic structure but also the microstructures [3]. In contrast to the X-ray diffraction patterns in previous work by Francisco J.A. et al. [15] and Campos Covarrubias M. S. et al. [16], the diffraction peaks in the present work are consistence with the pure phase of $Y_{0.1}BaCe_{0.9}O_3$ (YBC10).

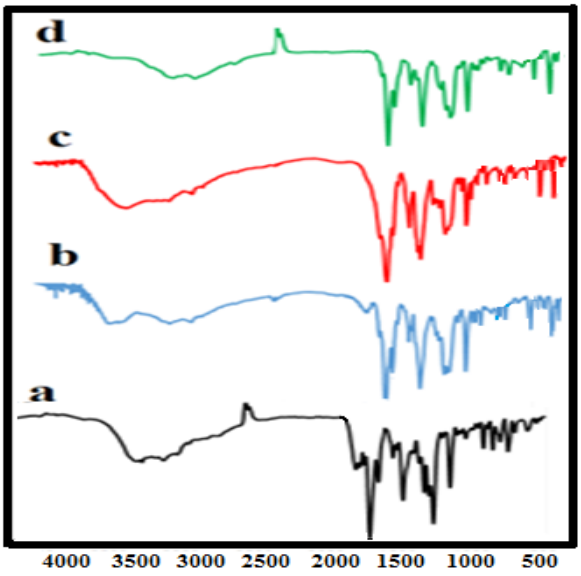

Fig. 1. FTIR spectra of a) LH2 ligand $[pyda.H2]^{2+}[pydc]^{2-}$, b) Y(III) complex $[(Y_2 (pydc)_4 (H_2O)_4].pyda.H]_2.2H_2O]]$, c) Ba(II) complex $\{[Ba_{1.5} (pydc.H) (pydc) (H_2O)]. H_2O. 0.5 (pydc.H2)\}_n$, and d) Ce(III) complex $[(Ce_2(pydc)_4(H_2O)_4].pyda.H]_2.2H_2O$.

As can be seen in Fig. 2, using the Debay-Scherrer formula ($D = 0.891\ \lambda/ß\cos\theta$), the average particle sizes have been calculated by the broadening of the XRD peaks where λ is the wavelength of X-ray radiation (1.541 Å), ß is the full width at half-maximum, and θ is the diffraction angle [17]. The average crystallite sizes calculated from the Debay-Scherrer formula were 22 and 46 nm for YBCO (I) and (II) powders, respectively. The peaks that appear between 20 and 30 in Fig 2 b) are related to BaO crystal lattices [16].

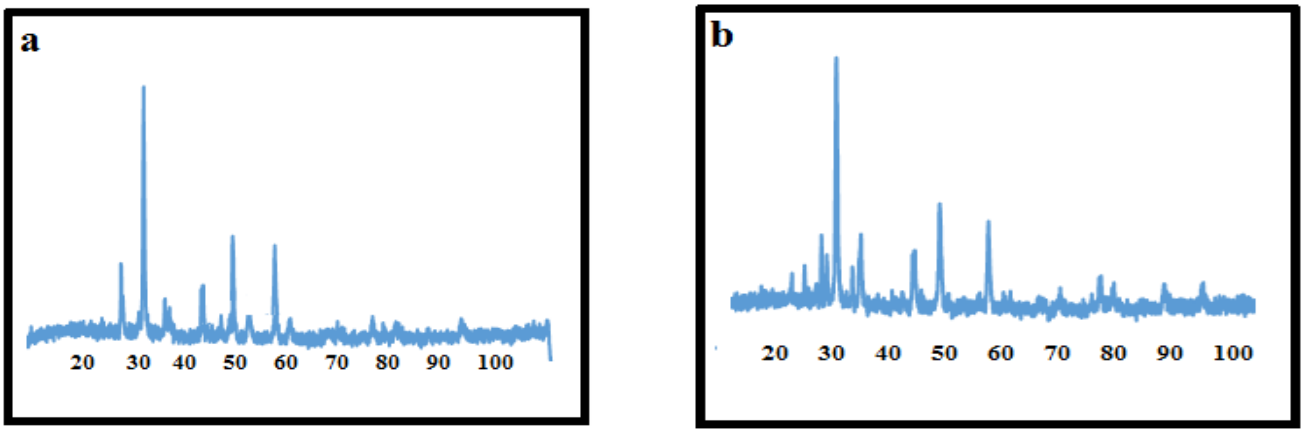

Fig. 2. The X-ray powder diffraction patterns of (a) YBCO (I) and b) YBCO (II).

The SEM micrographs of YBCO powders (I) and (II) are shown in Fig. 3. It can be seen that powders of YBCO contain many closed pores and few open pores. It can also be clearly observed in the micrographs that the samples have no cracks or deformation and that the samples exhibit a good grain. On the other hand, nonuniform grain growth with voids can be seen on the surface of the samples.

The SEM images of compounds (I) and (II) show a highly dense nano structure with some pores occurring from inhomogeneity (Fig. 3a, b) [18]. The powders synthesized with metal complexes containing LH_2 ligands are denser than those synthesized with metal salts as precursors under identical synthetic ruts and thermal treatments such as calcination and sintering conditions. According to the graphs, as the temperature increases, the grain sizes decrease, which explains why the grains' are less uniform in distribution and bimodal grain formations. Except for a few pores, the grain boundaries do not contain any secondary phases. The confinement of the anion vacancy to the oxygen site established for YBCO has considerable implications for the ionic conductivity of the doped barium cerates regardless of whether the conductivity is protonic or oxide ion mediated [19]. Additionally, growth in grain size between 59.96-112.86 and 132.79-221.32 nm for YBCO (I) and (II), respectively, can be seen (Fig. 3a, b). XRD measurements in Fig. 4 further confirmed the EDS analysis, which found that the compound consists of cerium, barium, and yttrium atoms.

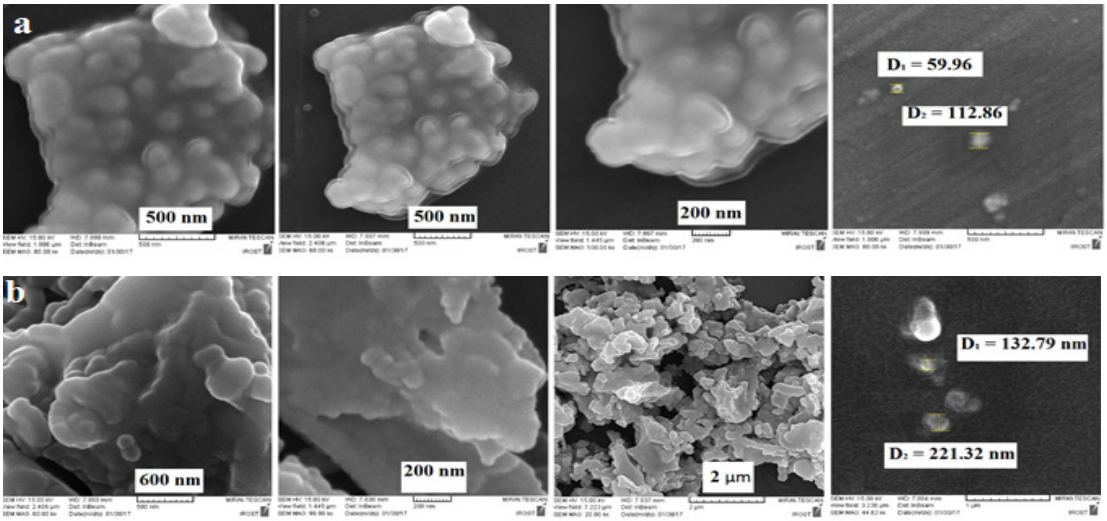

Fig. 3. SEM micrographs of (a) YBCO (I) and (b) YBCO (II).

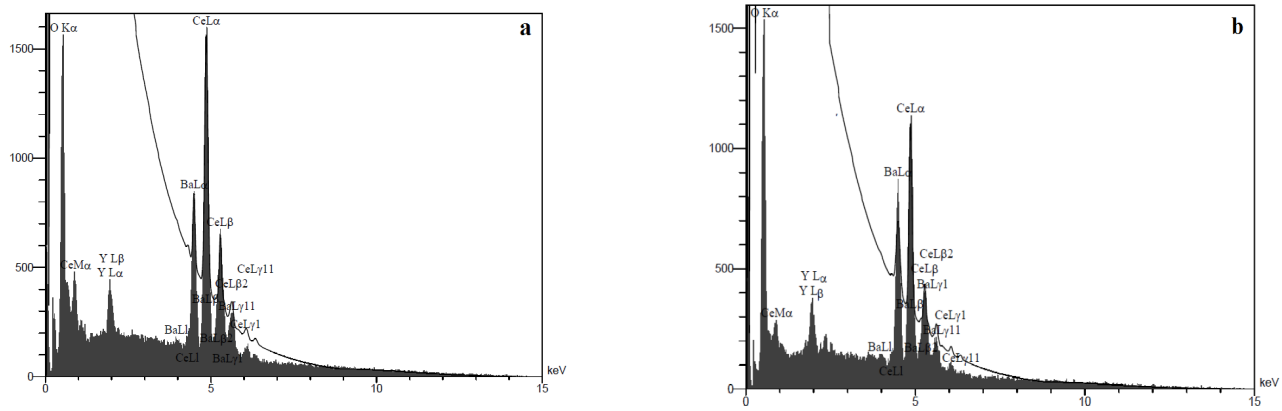

Fig. 4. EDS spectra of (a) YBCO (I) and (b) YBCO (II).

Figure 5 a and b show the TG curve for YBCO (I) and (II) powders from 25-1200 °C, respectively. The weight loss in the first steps corresponds to the removal of the structural water in the gel precursor. The weight loss in the second step corresponds to the combustion of inorganic and organic constituents of the precursors. The largest exothermic peak, observed in the final step, indicates the elimination of remaining organic materials, nitrates, and other unwanted compounds at this point.

Figure 6 shows the Nyquist plot of the electrochemical properties of both YBCO (I) and (II) at temperatures from 650 to 800 °C. The electrochemical impedance curve was performed under open-circuit conditions in the frequency range from 1 MHz to 0.1 Hz. Based on the results of impedance, it can be concluded that the morphology of the synthesized powder affects the ionic resistance of the electrolyte. Therefore, the function of the cell depends on the microstructure of the electrode and electrolyte [20].

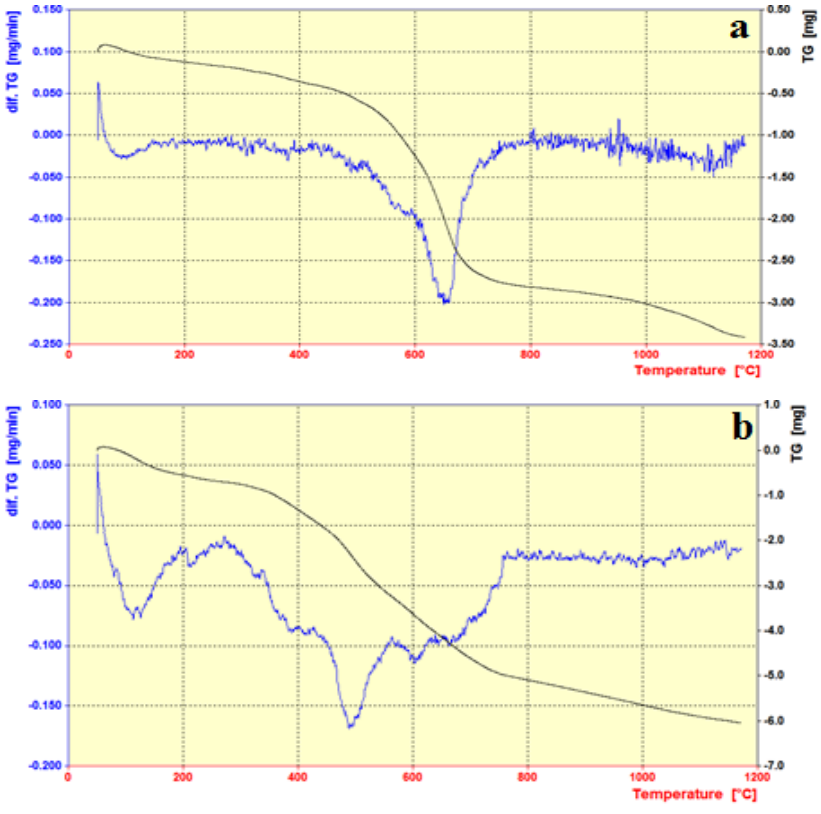

Fig. 5. TG/DTA diagrams of (a) YBCO (I) and (b) YBCO (II).

The microstructure of the electrode and the electrolyte is such that the length of the three-phase boundaries decreases then the function of the cell also degrades. The higher the resistance is at higher frequencies, the higher the intrusion/absorption process and the charge transitions due to the high porosity in the microstructure of the cell. From the results of the impedance shown in Fig. 6, it can be concluded that the morphology of the synthesized YBCO powder affects the ionized conductivity. As shown in the two examples of the Nyquist chart, the resistance level decreases because of the temperature increase from 650 to 800 °C. As the temperature increases, the ion conductivity in the samples increases as measured by the results of the impedance spectrum of YBCO (I) and (II).

However, the ionic conductivity of YBCO (I) is higher due to the improved microstructure of the YBCO electrolyte resulting from using new precursors. Since the total conductivity is equal to the aggregation of ion conduction and electrical conductivity, as the YBCO electrolytic conductivity increases, the total conductivity of the sample also soars because the only difference is the electrolyte structure. Therefore, the increasing overall resistance and weaker performance of YBCO (II), in comparison with YBCO (I), can be attributed to the poor connection of the particles and the weaker microstructure of the electrolytic powder of YBCO (II). Any problems with conducting of Ni, YBC, and fuel causes the electrochemical reactions not to be done. Therefore, in YBCO (II), it seems that there is no uniform or proper distribution at the sintering temperature between Ni and YBCO because we need high surface area, high porosity, and a good connection of electrode and electrolyte at the sintering temperature to have high-efficiency. Another likely reason is the reduction of the active electrochemical level between the cermet anode and electrolyte.

The presence of pores between the electrolyte and the anode (at the interface between the anode and the electrolyte) will reduce the length of the three-phase boundaries in electrochemical reactions [21]. The presence of pores must be within the structure of the anode since the fuel and the ions can easily pass through the structure. The presence of the pores at the joint level of the electrolyte and the anode reduces the length of the three-phase boundaries. It can be concluded that due to YBCO (I)'s better microstructure during sintering, greater cohesion between the anode and the electrolyte increases the common interface between them, which significantly reduces the resistance [22].

The activation energy of YBCO (I) and (II) was calculated considering the slope of the Arrhenius plots. The slopes of the Arrhenius plots (Fig. 7) of the Ln Rp decreased with the addition of new complexes to the YBCO (I). On this basis, we can conclude that the activation energy for the modified YBCO (I) was reduced. According to Fig. 7, the activation energy for YBCO (II) was 0.25 e.V, which decreased to 0.12 e.V for YBCO (I). Therefore, YBCO (II)'s connection between electrode and electrolyte was poor, but the addition of new complexes to YBCO (I) homogeneously distributed electrode and electrolyte and their interaction enhanced the electrical conductivity and lowered the activation energy.

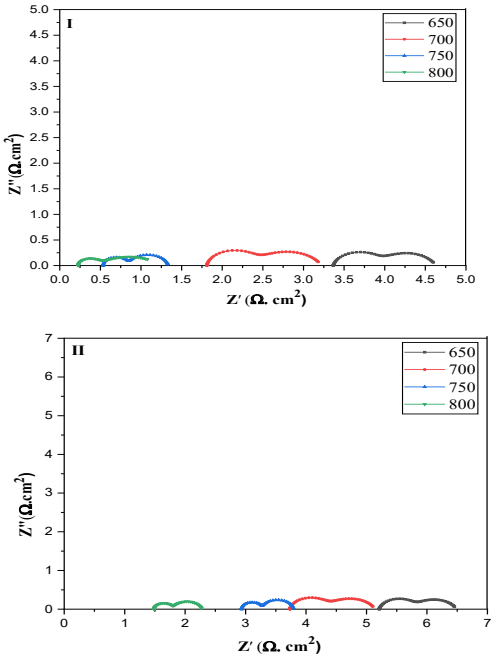

Fig.6. Polarization resistance values determined at temperatures from 650 to 800 °C for YBCO (I) and (II).

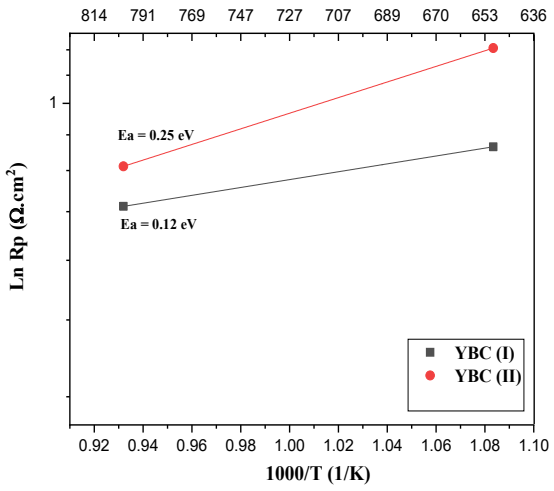

Fig 7. Arrhenius plot for YBCO (I) and (II) at temperatures of 650 and 800 °C.

4. Conclusions

In summary, in this study, we have successfully synthesized two different kinds of YBCO (I and II) nano composites using the sol–gel method. M-LH_2 containing supramolecular compounds and $M(NO_3)_x.XH_2O$, (M= Ce, Ba, Y) compounds were used as new precursors. The sol-gel method using metal complexes as precursors proved an effective technique for the preparation of a dense layer of YBCO electrolyte, as we proposed in this work. The study also found that the sono-chemical method can be employed successfully as simple, efficient, low-cost, environmentally friendly, and is very promising for the fabrication of nano-scale materials. The XRD confirmed the doping of ceria, and there were no secondary phases or peak representative of ytteria. In addition, it was possible to estimate the perovskite-type structure, ideal for proton ionic conductors such as solid oxide electrolyte applications. The SEM for the calcined powders at 900°C showed the strengthening of some agglomerates, which may hinder an ideal sintering process. The activation energy and resistance of YBCO (I) decrease with the addition of new complexes and shows good electrochemical performance due to the better microstructure of YBCO (I). Consequently, the results show that proton-conductive electrolytic powders (YBCs), after reforming by reducing the resistance and activation energy and increasing the efficiency, can be a good candidate for solid oxide fuel cell electrolytes.

Acknowledges

The Authors are grateful to the Iranian National Science Foundation (INSF) and the Iranian Research Organization for Science and Technology (IROSt).

References

[1] Kulkarni K., Duttagupta S., Phatak G., Preparation of Nano particle Core-Shell Electrolyte Materials for Proton, *Chem. Mater,* 22, 1119–1125, 2010.

[2] Khani Z., Taillades-Jacquin. M., Taillades G., Marrony M., Jones. D, Roziere. J, Sol–gel synthesis and protonic conductivity of yttrium doped, *J Sol-Gel Sci Technol,* 74, 94–102, 2015.

[3] Köferstein R., Hesse D., Ebbinghaus S., Synthesis and characterization of a nano scaled barium cerate perovskite powder using starch as polymerization agent, *Solid State Ionics,* 203, 52-56, 2011.

[4] Tenevich M., Pavlovich Shevchik A., Popkov V. I., Hydrazine-nitrate combustion synthesis of $BaCeO_3$

preceramic powders: structure, morphology and thermophysical properties, *Journal of Sol-Gel Science and Technology* 101, 380–389, 2022.

[5] Vanessa C. D. Graça,Francisco J. A. Loureiro,Laura I. V. Holz,Sergey M. Mikhalev, Duncan P. Fagg, Toward improved chemical stability of yttrium-doped barium cerate by the introduction of nickel oxide, *J. Am. Ceram.Soc.*; 105, 6271-6283, 2022.

[6] Tu C-S, Chien RR, Schmid VHt, Lee S-C, Huang C-C, Tsai C-L, Thermal stability of $Ba(Zr_{0·8-x}Ce_xY_{0·2})O_{2·9}$ ceramics in carbon dioxide, *J Appl Phys*, 105, 103504-103507, 2009.

[7] JunmengJing, JiePang, LiyanChen, HanZhang, ZeLei, ZhibinYang Structure, synthesis, properties and solid oxide electrolysis cells application of Ba(Ce, Zr)O_3 based proton conducting materialsChemical Engineering Journal, Volume 429, 1 February 2022, 132314

[8] Nasani, N., Dias, P. A. N., Saraiva, J. A., & Fagg, D. P., Synthesis and conductivity of Ba(Ce,Zr,Y) $O_{3-\delta}$ electrolytes for PCFCs by new nitrate-free combustion method. *International Journal of Hydrogen Energy*, 38, 8461-8470, 2013.

[9] Khani. Z, Taillades-Jacquin. M, Taillades. G, Marrony. M, Jones. D, Roziere. J, New synthesis of nanopowders of proton conducting materials. A routeto densified protonceramics, *Journal of Solid State Chemistry ,* 182, 790–798, 2009.

[10] Moghimi A., Ranjbar M., Aghabozorg H., Jalali F., Shamsipur M., Yap G.P.A., Rahbarnoohi H., "A novel pyridine containing self- assembling system: synthesis, charactrization, X-ray crystal structure, 13C solid phase NMR and solution studies, *J. Mol. Struct,* 605, 133-149, 2002.

[11] Ranjbar M., Mozaffari S.A., Kouhestanian E., Salaramoli H., Sonochemical synthesis and characterization of a Zn(II) supramolecule, bis(2,6 diamino- pyridinium) bis (pyridine-2,6-dicarboxylato)zincate(II), as a novel precursor for the ZnO-based dye sensitizer solar cell, *Journal of Photochemistry and Photobiology A Chemistry,* 321, 110-121, 2016.

[12] Ghamari. S, Ranjbar. M, Nabitabar. M, Preparation and characterization of nanopowder nickel oxide/ gadolinium-doped ceria via the sol-gel method by NiLH2 precursor, J Sol-Gel Sci Technol,81, 236–246, 2017.

[13] Matsumoto. H, Nomura. I, Okada. S, Ishihara, T, Matsumoto. H, Intermediate-temperature solid oxide fuel cells using perovskite-type oxide based on barium cerate, Solid State Ionics, 179, 1486–1489, 2008.

[14] Ła˛cz. A, Pasierb, P, Synthesis and properties of BaCe12xYxO3- δ –BaWO4 composite protonic conductors, J Therm Anal Calorim, 113, 405–412, 2013.

[15] Loureiro F.J.A., Ramasamy D., Ribeiro A.F.G., Mendes A., Fagg D.P., Electrochimica Acta 334, 135625-135633, 2020.

[16] Covarrubias M.S.C., Sriubas M., Vazgys R., Gazda M. Laukaitis G., Bockute K., Poskaite A., Appl. Sci., 12, 6422-6432, 2022.

[17] Zarkov. A, Stanulis. A, Salkus. T, Kezionis. A, Jasulaitiene. V, Ramanauskas. R, Tautkus. S, Kareiva. A, Synthesis of nanocrystalline gadolinium doped ceria via sol–gel combustion and sol–gel synthesis routes, Ceramics International, 42, 3977-3988, 2016

[18] Gu. J, He. L, Preparation of Y-doped Barium Cerate and Strontium Cerate Membranes, Key Engineering Materials, 280-283, 895-898, 2005.

[19] Knight. K. S, Soa. M, Bonanos. N, Crystal Structures of Gadolinium- and Yttrium-doped Barium Cerate, J. Mater. Chem. 2(7), 709-712, 1992.

[20] Ayawanna. J, Wattanasiriwech. D, Wattanasiriwech. S, Sato. K, Electrochemical Performance of $Ni_{1-x}Co_x$-GDC Cermet Anodes for SOFCs, Energy Procedia, 34, 439–448, 2013.

[21] Shi. N, Yu. Sh, Cen. S, Ge. L, Chen. H, Guo. L, Dense thin YSZ electrolyte films prepared by a vacuum slurry deposition technique for SOFCs, Ceramics International, 43, 182-186, 2017.

[22] Farrell. B, Linic. S, Direct electrochemical oxidation of ethanol on SOFC: Improved carbon tolerance of Ni anode by alloying, Applied Catalysis B: Environmental, 183, 386-393, 2016.